

N. T. Zinner · J. R. Armstrong · A. G. Volosniev ·  
D. V. Fedorov · A. S. Jensen

# Dimers, Effective Interactions, and Pauli Blocking Effects in a Bilayer of Cold Fermionic Polar Molecules

October 28, 2018

**Abstract** We consider a bilayer setup with two parallel planes of cold fermionic polar molecules when the dipole moments are oriented perpendicular to the planes. The binding energy of two-body states with one polar molecule in each layer is determined and compared to various analytic approximation schemes in both coordinate- and momentum-space. The effective interaction of two bound dimers is obtained by integrating out the internal dimer bound state wave function and its robustness under analytical approximations is studied. Furthermore, we consider the effect of the background of other fermions on the dimer state through Pauli blocking, and discuss implications for the zero-temperature many-body phase diagram of this experimentally realizable system.

## 1 Introduction

The cooling and trapping of ultracold polar molecules is a rapidly growing field at the moment [1, 2, 3, 4, 5, 6, 7], which generates huge theoretical interest [8, 9]. To avoid heavy losses from chemical reactions [7] or many-body collapse [10], trapping in low-dimensional geometries has been explored in multiple works [11, 12, 13, 14, 15, 16, 17, 18, 19, 20]. Very recently, a multilayer system of fermionic polar molecules was experimentally realized and chemical reactions rates that depend on the geometry and population of optical lattice states have been measured [21]. In addition to the potential for ultracold controlled chemistry of such a system, the long-range character of the dipole-dipole interaction means that the interactions of the molecules can potentially support a number of exotic few- and many-body phases [22, 23, 24, 25, 26, 27, 28, 29, 30, 31, 32, 33, 34, 35, 36, 37, 38, 39, 40, 41].

In the case of dipoles aligned perpendicular to the layers by an externally applied field the interaction of dipoles in different layers has a very interesting structure with short-range attraction and long-range repulsion. In fact, in momentum space the interaction becomes negative definite in the two-dimensional (2D) limit where the layers are assumed infinitely thin [23]. This suggests that the system could exhibit pairing. However, the intralayer interaction for the same alignment is purely repulsive [42], and this counteracts the pairing mechanism. This interplay of repulsive and attractive interactions in parallel planes is reminiscent of features in high-temperature superconductors and layers of cold polar molecules are therefore a very interesting model system.

Here we focus on the case of a bilayer which already contains many of the features expected of the general many-layer system. The two-dimensional two-component Fermi gas with attractive short-range interactions is a well-studied problem. In particular, the interesting physics of the BCS-BEC crossover from weakly paired atoms to strongly bound dimers was obtained some years ago [43, 44, 45]. It was shown that the crossover takes place when the Fermi energy of the system becomes comparable to the binding energy of the two-body bound state between the two components (typically electron spins) of the generic Fermi gas. The existence of the latter state is guaranteed by the famous Landau criterion

which states that a potential with a negative definite volume integral always supports a bound state [46]. A bilayer with fermionic polar molecules is similar to the 2D Fermi gas when mapping the spin to a layer index. The important role of the two-body bound state in the many-body physics of the bilayer is now clear.

The bilayer setup with perpendicular dipole moments has a two-body bound state which is supported by the interlayer potential whose inner part is the only source of attraction. However, the spatial integral of the potential turn out to be zero and Landau's criterion cannot be applied to secure a bound state at any coupling strength of the dipolar molecules. An early proof of the existence of a bound state even for vanishing spatial integral was given by Simon [47]. In the initial stages of the theoretical work on dipolar systems in 2D, this result appears to have been forgotten and Gaussian approximations that predict a critical coupling strength for a bound two-body state to arise were used [48, 15, 22, 28]. The energy of the bound state for the interlayer potential of a bilayer with perpendicular dipoles was first calculated within a scattering approach in [49] and by solving the Schrödinger equation in [50, 54]. The highly non-trivial dependence of the bound state energy on the coupling strength was subsequently calculated for perpendicular [55, 56, 34], and for arbitrary orientation of the dipoles with respect to the planes [57].

In this paper we consider the properties of the two-body bound dimer for dipolar fermions in a bilayer with dipoles oriented perpendicular to the layers. The exact binding is obtained by numerical solution of the Schrödinger equation and different approximation schemes based on Gaussian and exponential wave functions are tested against the exact result. The momentum-space wave function is then calculated and used to discuss an effective dimer-dimer interaction for use in the corresponding many-body problem. Here we find that appropriate Gaussian wave functions provide good analytic approximations to the exact result everywhere except the weak-coupling limit where the wave function becomes very delocalized in space. Lastly, we consider the bound state in the context of the BCS-BEC crossover. We include the Pauli blocking effect of the fermionic background by solving the momentum-space Schrödinger equation and compare to a Gaussian approximation scheme. The binding energy of the dimer is found to decrease rapidly with increasing size of the background Fermi sea. The latter means that the (quasi)-BEC regime where the system effectively consists of bound dimers occupies only a small region of the phase diagram at very low density, making it hard to reach experimentally.

## 2 Model

We consider the case of a bilayer geometry with a single polar molecule of mass  $M$  and dipole moment  $\mathbf{d}$  in each layer. We assume the molecules are fermions, but this will only play a role later when considering the effect of Pauli blocking on the binding energy. We assume that the dipole moments have been aligned by an external field so that they are oriented perpendicular to the layers in which the molecules move. In this setup the dipolar potential is

$$V(r) = D^2 \frac{r^2 - d^2}{(r^2 + d^2)^{5/2}}, \quad (1)$$

where  $d$  is the interlayer distance and  $D^2 = \mathbf{d}^2/4\pi\epsilon_0$  (assuming electric dipole moments,  $\mathbf{d}$ ). The three-dimensional distance between the molecules is  $r^2 + d^2$ , i.e.  $r$  is the relative distance in the plane. For  $r/d \ll 1$  the potential behaves as an oscillator, whereas for  $r/d \gg 1$  it has a repulsive  $1/r^3$  tail. Note the interesting feature that  $\int d^2\mathbf{r}V(\mathbf{r}) = 0$ , which implies a highly non-trivial behavior of the binding energy for small dipole moments [47, 50, 55, 54, 34, 57, 56].

Since the potential has cylindrical symmetry, the two-body Schrödinger equation can be decomposed into partial waves  $\Psi(r) = \sum_m R_m(r)\psi_m(\phi)$  with radial equation

$$-\frac{\hbar^2}{2\mu} \left( \frac{d^2}{dr^2} + \frac{1 - 4m^2}{4r^2} \right) u_m(r) + V(r)u_m(r) = Eu_m(r), \quad (2)$$

where  $\mu = M/2$  is the reduced mass and  $u_m(r) = \sqrt{r}R_m(r)$  is the reduced radial wave function. In this paper we will only be concerned with the lowest  $m = 0$  state which yields the radial equation

$$\left[ \frac{d^2}{dx^2} + \frac{1}{4x^2} - U \frac{x^2 - 2}{(x^2 + 1)^{5/2}} + \tilde{E} \right] u_0(x) = 0, \quad (3)$$

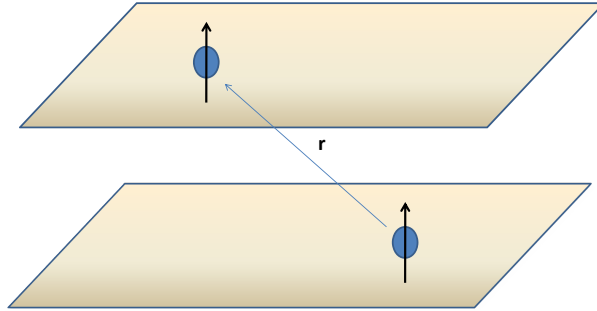


**Fig. 1** (color online) Schematic picture of the bilayer setup with one dipolar molecule in each layer at distance  $r$ . The dipole moment is polarized perpendicular to the bilayer planes by an externally applied field.

where we have rescaled the equation to dimensionless units, i.e.  $x = r/d$  and  $\tilde{E} = Md^2E/\hbar^2$ . The dimensionless strength of the dipolar interaction in the bilayer setup is  $U = MD^2/\hbar^2d$ . Unless otherwise stated, we will use  $\hbar^2/Md^2$  as the unit of energy and  $d$  for lengths.

The two-body Schrödinger equation in Eq. (3) can be solved numerically by standard methods. We denote the exact energy obtained from solving this equation by  $E_0$  and the wave function by  $\Psi_0$ . However, when the dimer appears as input for more involved calculations on the many-body physics of layered systems, it is extremely useful to have accurate analytic or semi-analytic approximations to the full wave function. This will be our main concern in this paper, and we now outline four approximation schemes that we want to compare. The first three are based on an increasingly more sophisticated oscillator approximation, whereas the last one is an exponential ansatz for the wave function. What will be evident is that it is very important for any approximation to properly reproduce the spatial profile of the wave function.

## 2.1 Scheme 1

The simplest and also crudest approximation is to expand the potential to quadratic order for  $r \ll d$ ,

$$V(r) \approx -\frac{2D^2}{d^3} + \frac{1}{2} \frac{12D^2}{d^5} r^2, \quad (4)$$

which yields the relation  $\mu\omega^2 = \frac{12D^2}{d^5}$  for the angular frequency of the oscillator. The corresponding wave function is simply

$$\Psi_1(r) = \frac{1}{\sqrt{\pi}b} e^{-\frac{r^2}{2b^2}}, \quad (5)$$

where  $b^2 = \hbar/\mu\omega$ . As we will see below, this gives a bad estimate for the binding energy, but does exhibit some of the right behavior for large  $U$  where the wave function localizes and becomes increasingly Gaussian. We denote the energy and wave function obtained from this first approximation scheme by  $E_1$  and  $\Psi_1$ . Recall that for Gaussian wave functions with parameter  $b$  in two dimensions we have  $\langle r^2 \rangle = b^2$ .

## 2.2 Scheme 2

Another strategy is to use the nice Gaussian wave function but employ the oscillator length corresponding to the correct binding energy. The relation between binding energy,  $E_B$ , and oscillator length parameter,  $l$ , is  $l^2 = 2\hbar^2/ME_B$ . We now take  $E_B = |E_0|$ , i.e. we use the *exact* result for the energy

to determine the length scale of the Gaussian ground-state wave function  $\Psi_2$ . This has the advantage that the wave function will become increasingly extended for small  $U$  and, in turn, small  $|E_0|$ .

### 2.3 Scheme 3

The third use of Gaussian approximation schemes is somewhat more involved and builds on ideas discussed earlier in Ref. [50]. We approximate the true potential by a model potential which is quadratic but with a constant (negative) shift. We then fit the oscillator frequency and the shift to ensure that (i) the binding energy is equal to the exact result and (ii) the node of the potential occurs at  $r/d = \sqrt{2}$  which is the same position as for the real potential in Eq. (1). The latter condition reflects the idea that the inner attractive part is the important one that determines the properties of the system, whereas the outer repulsive tail of the true dipolar interaction has only limited influence. Assuming a potential of the form  $V(r) = M\tilde{\omega}^2 r^2/4 - E_s$ , the two conditions yield the following matching relations between angular frequency,  $\tilde{\omega}$ , shift,  $E_s > 0$ , and  $E_0$

$$\frac{1}{2}Md^2\tilde{\omega}^2 = E_s \quad \text{and} \quad E_0 = \hbar\tilde{\omega} - E_s. \quad (6)$$

These second order equations have two solutions

$$x_{\pm} = 1 \pm \sqrt{1 - 2\tilde{E}_0}, \quad (7)$$

where  $x_{\pm} = Md^2\tilde{\omega}_{\pm}/\hbar$  and  $\tilde{E}_0 = Md^2E_0/\hbar^2$ . The solutions have the properties that  $x_+ \rightarrow 2 - E_0$  and  $x_- \rightarrow E_0$  for  $|E_0| \rightarrow 0$ . We see that the  $x_+$  solution goes to a constant oscillator frequency, whereas the  $x_-$  goes to a vanishing frequency. The approximating potential becomes

$$V(r) = \left(x_{\pm} - \frac{Md^2E_0}{\hbar^2}\right) \left[\frac{1}{2}\left(\frac{r}{d}\right)^2 - 1\right], \quad (8)$$

where since  $E_0 < 0$  the first factor is always positive and tends to zero for  $|E_0| \rightarrow 0$  in the weak-coupling limit. The solution  $x_-$  is negative, and therefore  $\tilde{\omega}_- = \hbar x_-/Md^2 < 0$ . Therefore this quantity cannot be interpreted as an oscillator frequency as it stands. However, if we take  $\tilde{\omega}_- = \hbar|x_-|/Md^2$ , we get a positive frequency which has the desirable feature that the wave function is allowed to extend in space when  $|E_0|$  is small. The price we pay is that now the binding energy in the oscillator is not equal to the exact result,  $E_0$ , but becomes

$$Md^2\tilde{\omega}_-/\hbar - Md^2E_s/\hbar^2 = 2\sqrt{1 - 2\tilde{E}_0} + \tilde{E}_0 - 2, \quad (9)$$

in dimensionless form. The energy in the  $\tilde{\omega}_-$  oscillator is then positive for  $-\tilde{E}_0 < 4$ , but still goes to zero as  $|E_0| \rightarrow 0$ . Since it is highly desirable to have an extended potential (i.e.  $\tilde{\omega}_- \rightarrow 0$ ) as  $|E_0| \rightarrow 0$  we retain this solution despite the difference in ground state energy. The length scale of the Gaussian ground-state of the  $\tilde{\omega}_{\pm}$  oscillators has the simple form  $l^2/d^2 = 2/|x_{\pm}|$ , which clearly diverges as  $|E_0| \rightarrow 0$  for the  $\tilde{\omega}_-$  solution. We denote the corresponding wave function  $\Psi_3$ .

Below we will see that whereas the approximation using  $\tilde{\omega}_-$  compares poorly with exact results, using  $\tilde{\omega}_+$  gives a much better approximation in spite of its localized behaviour when approaching zero energy ( $x_+ \rightarrow 2$ ). The approximation with  $\tilde{\omega}_+$  has been used to calculate the bound state energy of chains with one molecule in each layer in the three- and four-layer cases, and yields results that are in excellent agreement with exact numerical methods [51, 52, 53].

### 2.4 Scheme 4

The final approximation scheme uses an exponential wave function instead of a Gaussian but still uses the exact binding energy. This means that we reproduce the correct large-distance behavior of the

exact wave function. The wavenumber  $\kappa$  of the exponential is fixed similar to approximation scheme 2, i.e.  $|E_0| = \hbar^2 \kappa^2 / 2\mu$  or  $\kappa = \sqrt{M|E_0|/\hbar^2}$ . The properly normalized wave function for this scheme is

$$\Psi_4(r) = \sqrt{\frac{2}{\pi}} \kappa e^{-\kappa r}. \quad (10)$$

For this wave function we have  $\langle r^2 \rangle = 3/2\kappa^2$ . Scheme 4 is special in the sense that it is designed to approximate the tail behavior of the full wave function. Since the exponential form is not correct at small distances it does not make sense to calculate the energy for this wave function. The correct wave function for bound states outside the range of the potential in two dimensions is the modified Bessel function of the second kind  $K_0$ , which does have the exponential tail but is logarithmically divergent at the origin.

### 3 Dimer Properties

We now compare the properties of the exact dimer solution from the Schrödinger equation to the various approximation schemes introduced above. We do this for the energy obtained in scheme 1, and for the wave function and radius squared for all schemes. Furthermore, we consider the Fourier transform of the wave functions and of their square which will be of use when discussing the effective interaction of dimers below.

#### 3.1 Binding Energy

The first property of the dimer system to study is the binding energy. Since the ground-state has cylindrical symmetry, the exact solution can be obtained by integrating the Schrödinger equation and matching to a bound state wave function at large distances. This energy has been calculated by several groups in recent years [49, 50, 55, 34, 57]. In Fig. 2 the energy,  $E_0$ , is plotted as a function of the dipolar strength  $U$ . At very small  $U \sim 1$  one sees the rapid decrease of the binding energy which to leading order goes as  $e^{-8/U^2}$  [47, 55, 34, 57, 56]. The calculation was done for  $U \geq 0.9$  as smaller  $U$  values have binding energies that were below the numerical precision. Note that the exact energy is recovered by definition in approximation schemes 2 and 3 above ( $E_2 = E_3 = E_0$ ).

Also shown in Fig. 2 is the result of calculating the energy by a crude harmonic approximation to the potential around  $r = 0$ . The energy has the following analytical expression

$$\frac{Md^2}{\hbar^2} E_1 = \sqrt{24U} - 2U. \quad (11)$$

For  $U < 6$  we find  $E_1 > 0$ . This is of course due to the zero-point energy which is very large in this particular approximation. However, at larger  $U$  we do see the correct slope of  $E_1$  as compared to the exact result, and the difference seems to be only an overall offset. This clearly indicates that approximating the wave function by a Gaussian should be an accurate description for larger  $U$  as noted in [50]. It is of course clear that this tight harmonic approximation will fail at small  $U$ . To remedy this situation, we now discuss a number of alternative approximations to the wave function which use knowledge of the exact result, but where the scale of the wave function varies with  $U$  in a different way as compared to the crude harmonic approximation of  $\Psi_1$ .

First, we check the energies calculated within the various approximation that are based on Gaussians where a nice analytical expression can be given for the total energy. In fact, we have

$$\frac{Md^2}{\hbar^2} \langle H \rangle = x^2 [1 - Uf(x)], \quad (12)$$

$$f(x) = -4x^2 + 2\sqrt{\pi} \text{Erfc}(x) e^{x^2} (2x^3 + x), \quad (13)$$

where  $\text{Erfc}(x)$  is the complementary error function. We used the quantity  $x = d/b$ , where  $b$  is the length parameter in the Gaussian wave function. The optimal variational energy is now found by finding the minimum of Eq. 12 with respect to  $x$ . This value can be compared to the choices of length parameter

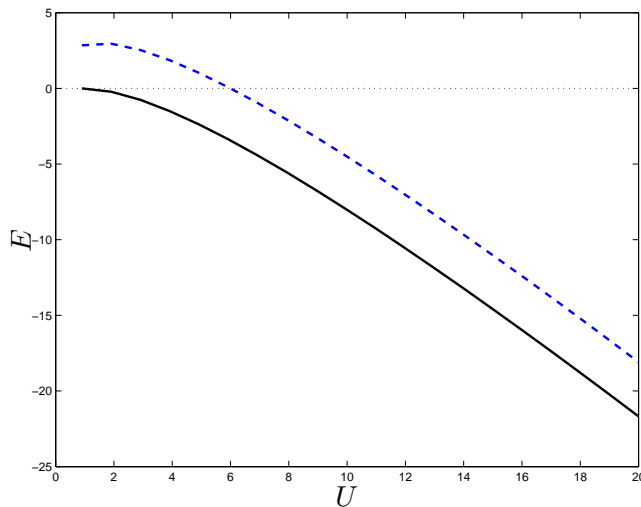


**Fig. 2** (color online) Dimer energy as a function of  $U$  in units of  $Md^2/\hbar^2$  for  $U \geq 0.9$ . The solid (black) line is the exact solution ( $E_0$ ), whereas the dashed (blue) line is the energy obtained by expanding the dipolar potential around the origin to second order in approximation scheme 1 ( $E_1$ ). The horizontal dotted (black) line indicates zero energy.

based on the exact energy and the shape of the potential as outlined in approximation schemes 2 and 3. We have chosen not to list this approximation among the schemes above since it is not based on the knowledge of the binding energy for construction of the wave function which is what the comparison done here is about. The variational approach provides both a binding energy and a corresponding (Gaussian) wave function, which is as we will now see close to some of the other schemes.

In Fig. 3 we plot the energies of the different Gaussian approaches along with the exact energy and also the energy result of the crude approximation in scheme 1. Note that all approximate solutions have positive energy below  $U \sim 1.5$ . Comparing the solid (red) and dashed (black) curves we see that the variationally optimized solution is better than scheme 2 but not by a large margin, and the difference becomes small for large  $U$  where they both approach the exact result. The two dotted (green) curves from scheme 3 are interesting as  $\tilde{\omega}_-$  seems to do consistently worse than  $\tilde{\omega}_+$ , with the exception of small  $U$  where the  $\tilde{\omega}_+$  solution goes positive. Note how scheme 2 and scheme 3 with  $\tilde{\omega}_+$  does well in the large  $U$  and small  $U$  regimes respectively, where they agree also with the variational calculation.

### 3.2 Wave function and Size

Next we look at the wave function of the exact solution in comparison to the different approximation schemes. In Fig. 4 we plot all the different choices for strengths  $U = 1, 2, 5,$  and  $10$ . As expected, scheme 1 is poor for small  $U$  and only becomes acceptable around  $U = 10$ , while the exponential approximation to the wave function is quite good in all cases. The former scheme simply can not deal with a rapid spreading of the wave function at small  $U$ . For schemes 2 and 3 we see quite good agreement with scheme 2 always giving a slightly better approximation.

From the wave function we can determine the extension of the dimers in the various approximation by computing  $\langle r^2 \rangle$ . The results are shown in Fig. 5 on a logarithmic scale which is convenient since at  $U \sim 1$  the dimer becomes extremely extended. Again we see that the exponential form in scheme 4 does remarkably well, whereas scheme 2 and 3 overestimate the size for  $U \gtrsim 2.5$ . Scheme 1 has a very small radius for all  $U$  and is quite far off the exact result as was clear from the wave functions in Fig. 4. It is worth noting that all curves in Fig. 5 have similar decreasing behavior for large  $U$  although the asymptotic values are very different. It is also interesting that even though the exact result predicts a dimer of size less than the attractive part of the potential for  $U \gtrsim 4$ , scheme 1 does not provide a good size estimate until much larger  $U$  even though it was built on only this inner attractive harmonic part of the full dipole-dipole potential. The lowest order expansion is therefore clearly insufficient.

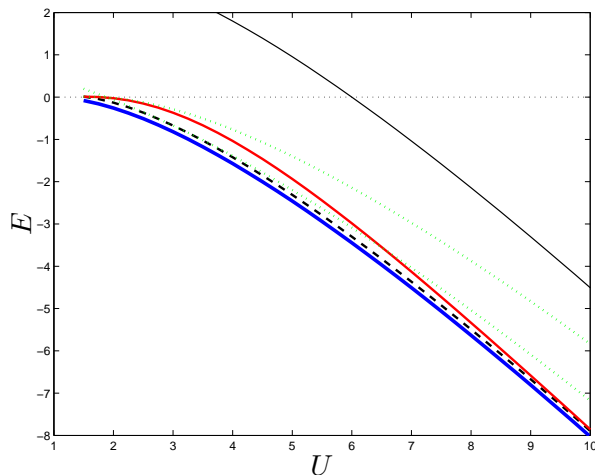


**Fig. 3** (color online) Dimer energy as a function of  $U$  in units of  $Md^2/\hbar^2$  for  $U \geq 0.9$ . The thick solid (blue) line is the exact solution ( $E_0$ ) and the upper thin solid (black) line is the energy obtained by expanding the dipolar potential around the origin to second order in approximation scheme 1 ( $E_1$ ). The solid (red) line is the energy based on the choice of length parameter in scheme 2, while the dashed (black) line is the optimum variational choice when using a Gaussian wave function. The two dotted (green) lines are for scheme 3 with the lower curve at large  $U$  corresponding to  $\tilde{\omega}_+$  and the upper one to  $\tilde{\omega}_-$ . The vertical dotted (black) line indicates zero energy.

From the results above, we can conclude that the key issue to obtain a good approximation seems to be the choice of bound-state size. Schemes 2 and 4 which includes only the size estimated through the binding energy are always the more accurate choices, with scheme 3 which includes the zero of the original potential also doing well. The naive harmonic approximation to the potential seems to fail in all aspects as seen in Figures 3, 4, and 5.

### 3.3 Fourier Transforms

Below we are concerned with the effective interaction between dimers which can be calculated from the Fourier transform of the dimer wave function. We define the Fourier transform to momentum space as

$$\tilde{\Psi}(\mathbf{k}) = \int d^2\mathbf{x} e^{-i\mathbf{k}\cdot\mathbf{x}} \Psi(\mathbf{x}). \quad (14)$$

Since the wave function has cylindrical symmetry we can perform the angular integration and obtain

$$\tilde{\Psi}(k) = 2\pi \int dx x J_0(kx) \Psi(x), \quad (15)$$

where  $J_0(z)$  is the Bessel function of order zero. For the Gaussian wave function,  $\Psi(x) = e^{-x^2/2b^2}/\sqrt{\pi b^2}$ , the result is

$$\tilde{\Psi}(k) = 2\sqrt{\pi} b e^{-k^2 b^2/2}, \quad (16)$$

while the exponential,  $\Psi(x) = \sqrt{2/\pi} \kappa e^{-\kappa x}$ , yields

$$\tilde{\Psi}(k) = 2\sqrt{2\pi} \frac{\kappa^2}{(k^2 + \kappa^2)^{3/2}}. \quad (17)$$

The remarks made about the various approximation schemes in coordinate space in relation to Fig. 4 hold for the Fourier transforms as well with scheme 1 doing quite bad while scheme 2,3, and 4 comparing much better with the exact result.

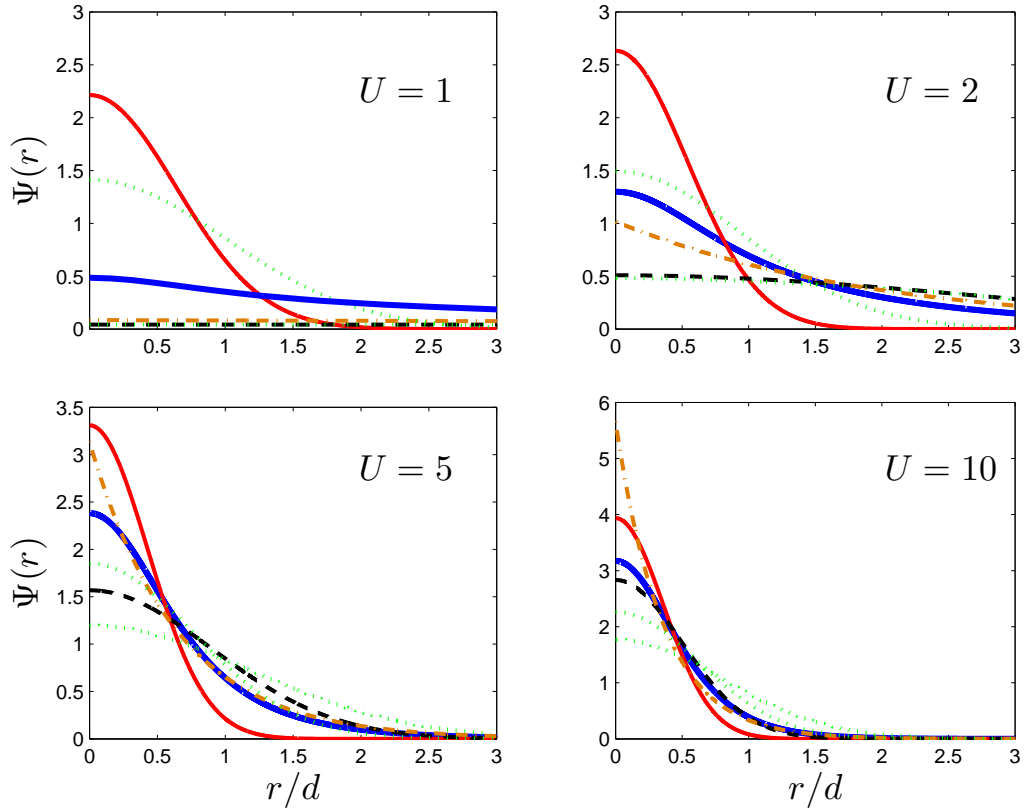


**Fig. 4** (color online) Dimer radial wave function for  $U = 1, 2, 5$  and  $10$ , in units of  $Md^2/\hbar^2$ . The solid thick (blue) line is the exact solution. The other lines are approximation scheme 1 (solid red), 2 (dashed black), 3 (dotted green), and 4 (dash-dotted brown). Note the difference in scales on the vertical axis. The upper (at  $r = 0$ ) dotted green corresponds to  $\tilde{\omega}_+$  in scheme 3 and the lower one to  $\tilde{\omega}_-$ .

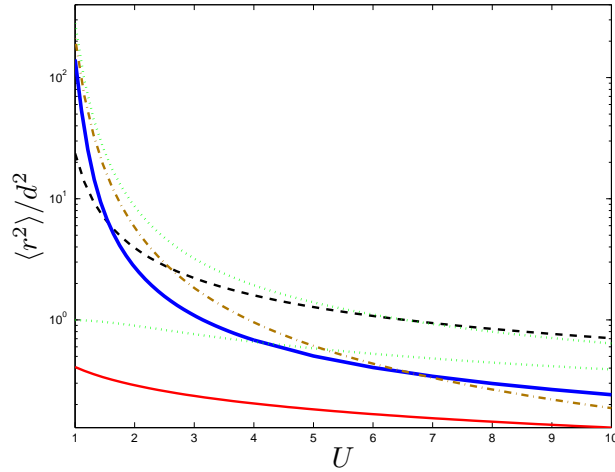


**Fig. 5** (color online) Mean radius squared,  $\langle r^2 \rangle$ , as function of  $U$  on a logarithmic scale. The lines are as in Fig. 4. The upper (at  $U = 1$ ) dotted (green) line corresponds to  $\tilde{\omega}_-$  and the lower one to  $\tilde{\omega}_+$  within scheme 3.



## 4 Effective Dimer-Dimer Interaction

We now turn our attention to the evaluation of an effective dimer-dimer interaction that takes both intra- and inter-layer interactions into account and uses the full dimer wave function as well. This procedure was discussed in [32] within the approximation scheme 2 outlined above. Here we elaborate and present a full comparison of various approximation and the influence on the effective dimer-dimer interaction.

### 4.1 Derivation

Consider two dimers in a bilayer. Let the coordinates of the polar molecules in each layer be  $\mathbf{r}_1, \mathbf{r}_2$  in the first dimer and  $\mathbf{r}_3, \mathbf{r}_4$  in the second dimer. Define the coordinates relative coordinates  $\mathbf{r} = \mathbf{r}_1 - \mathbf{r}_2$  and  $\mathbf{r}' = \mathbf{r}_3 - \mathbf{r}_4$ , and the center-of-mass (CM) for each dimer,  $\mathbf{R} = (\mathbf{r}_1 + \mathbf{r}_2)/2$  and  $\mathbf{R}' = (\mathbf{r}_3 + \mathbf{r}_4)/2$ . The distance between the CM of the two dimers is  $\boldsymbol{\rho} = \mathbf{R} - \mathbf{R}'$ . The effective potential is obtained by integrating over the wave function of the dimers and over the CM coordinates with the condition that  $\boldsymbol{\rho} = \mathbf{R} - \mathbf{R}'$  (we specify the meaning of this below). We have

$$V_{eff}(\boldsymbol{\rho}) = \int d\mathbf{r}d\mathbf{r}'d\boldsymbol{\rho}' |\Psi(\mathbf{r}_1, \mathbf{r}_2, \mathbf{r}_3, \mathbf{r}_4)|^2 \times \\ [V_{\text{dip}}(\mathbf{r}_1 - \mathbf{r}_2) + V_{\text{dip}}(\mathbf{r}_3 - \mathbf{r}_4) + V_{\text{dip}}(\mathbf{r}_1 - \mathbf{r}_3) \\ V_{\text{dip}}(\mathbf{r}_1 - \mathbf{r}_4) + V_{\text{dip}}(\mathbf{r}_2 - \mathbf{r}_3) + V_{\text{dip}}(\mathbf{r}_2 - \mathbf{r}_4)], \quad (18)$$

where  $V_{\text{dip}}$  is the dipole potential in coordinate-space and  $\Psi$  is the total wave function of the system. Here we have defined the total center-of-mass coordinates of all four molecules,  $\boldsymbol{\rho}' = (\mathbf{R} + \mathbf{R}')/2$ . For the latter we assume

$$\Psi(\mathbf{r}_1, \mathbf{r}_2, \mathbf{r}_3, \mathbf{r}_4) = \phi(\mathbf{r})\phi(\mathbf{r}')\psi(\mathbf{R})\psi(\mathbf{R}'), \quad (19)$$

where  $\phi$  is the relative wave function and  $\psi$  is the center-of-mass wave function of the dimers. We expect this to be a good approximation for a system of many particles when the dimer is strongly bound for large  $U$  and can be considered the effective constituent. We can write

$$V_{eff}(\boldsymbol{\rho}) = \int d\mathbf{r}d\mathbf{r}'d\boldsymbol{\rho}' |\phi(\mathbf{r})|^2 |\phi(\mathbf{r}')|^2 \times \\ |\psi(\mathbf{R})|^2 |\psi(\mathbf{R}')|^2 \left[ V_{\perp}(\mathbf{r}) + V_{\perp}(\mathbf{r}') + V_{\parallel}(\boldsymbol{\rho} + \frac{\mathbf{r} - \mathbf{r}'}{2}) \right. \\ \left. V_{\parallel}(\boldsymbol{\rho} - \frac{\mathbf{r} - \mathbf{r}'}{2}) + V_{\perp}(\boldsymbol{\rho} + \frac{\mathbf{r} + \mathbf{r}'}{2}) + V_{\perp}(\boldsymbol{\rho} - \frac{\mathbf{r} + \mathbf{r}'}{2}) \right], \quad (20)$$

where  $V_{\perp}$  is the inter-layer dipole potential and  $V_{\parallel}$  is the intra-layer dipole potential. Assume now that the center-of-mass part is proportional to  $\delta(\mathbf{R} - \mathbf{R}' - \boldsymbol{\rho})\delta((\mathbf{R} + \mathbf{R}')/2 - \mathbf{R}_{\text{CM}})$ , where  $\mathbf{R}_{\text{CM}}$  is the center-of-mass position of the total four-body system which is unimportant here (we can fix the coordinate system so that  $\mathbf{R}_{\text{CM}} = 0$  in any case). One can then drop the center-of-mass part of the integral. Likewise, the integral over the first two potential terms gives the potential energy of the dimer which is a constant that can be discarded. We are left with

$$V_{\text{eff}}(\boldsymbol{\rho}) = \int d\mathbf{r}d\mathbf{r}' |\phi(\mathbf{r})|^2 |\phi(\mathbf{r}')|^2 \left[ V_{\parallel}(\boldsymbol{\rho} + \frac{\mathbf{r} - \mathbf{r}'}{2}) \right. \\ \left. + V_{\parallel}(\boldsymbol{\rho} - \frac{\mathbf{r} - \mathbf{r}'}{2}) + V_{\perp}(\boldsymbol{\rho} + \frac{\mathbf{r} + \mathbf{r}'}{2}) + V_{\perp}(\boldsymbol{\rho} - \frac{\mathbf{r} + \mathbf{r}'}{2}) \right]. \quad (21)$$

The Fourier transform is given by

$$\begin{aligned}
 V_{\text{eff}}(\mathbf{k}) &= \int V_{\text{eff}}(\boldsymbol{\rho}) \exp^{-i\mathbf{k}\cdot\boldsymbol{\rho}} d\boldsymbol{\rho} = \\
 &\int d\mathbf{r}d\mathbf{r}' |\phi(\mathbf{r})|^2 |\phi(\mathbf{r}')|^2 \left[ 2V_{\parallel}(\mathbf{k}) \cos\left(\mathbf{k} \cdot \frac{\mathbf{r} + \mathbf{r}'}{2}\right) \right. \\
 &\quad \left. + 2V_{\perp}(\mathbf{k}) \cos\left(\mathbf{k} \cdot \frac{\mathbf{r} - \mathbf{r}'}{2}\right) \right], \tag{22}
 \end{aligned}$$

where  $V_{\parallel}(\mathbf{k})$  is the intra-layer and  $V_{\perp}(\mathbf{k})$  is the inter-layer momentum-space potential respectively.

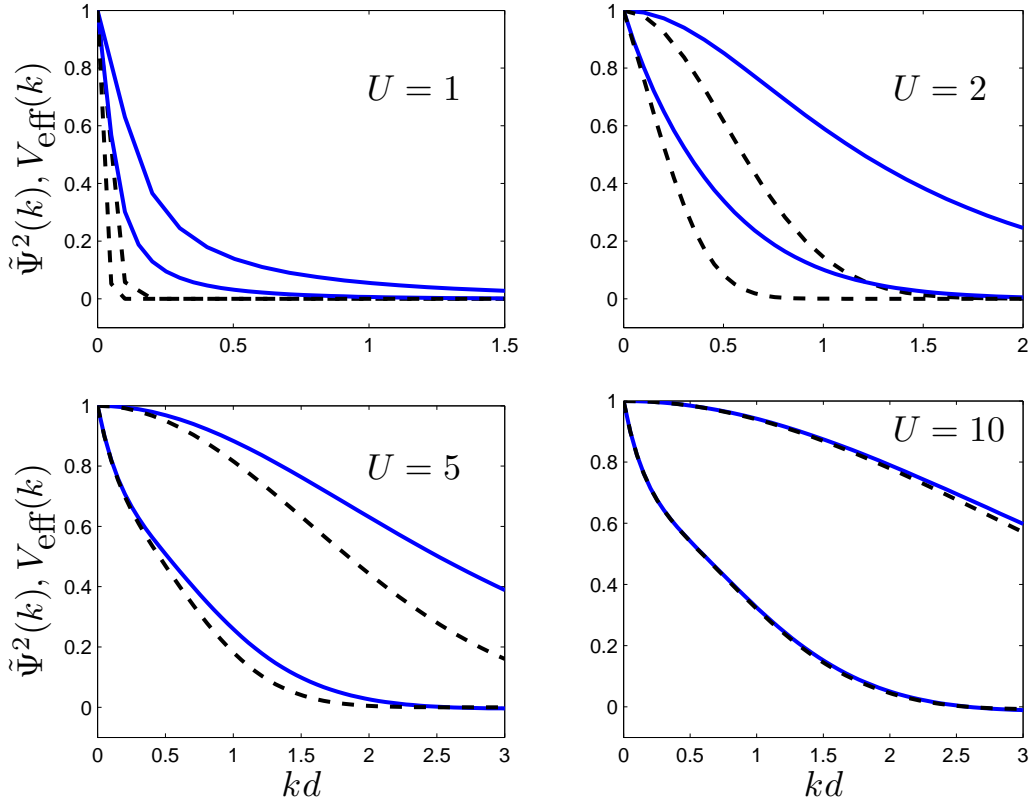


**Fig. 6** (color online) Plot of the (normalized) effective dimer-dimer interaction,  $V_{\text{eff}}(k)/V_{\text{eff}}(0)$ , along with  $\tilde{\Psi}^2(k)$  for  $U = 1, 2, 5,$  and  $10$ , and with layer width  $w/d = 0.1$ . The lower of the two solid lines is the effective potential while the upper one is  $\tilde{\Psi}^2(k)$  (and likewise for the dashed lines). The solid (blue) lines use the exact dimer wave function, whereas the dashed (black) lines are within the Gaussian approximation scheme 2. Note the differences in the horizontal scale of the panels.

The explicit expression for the interaction potentials in momentum space are

$$V_{\parallel}(\mathbf{q}) = \frac{8\pi D^2}{3\sqrt{2\pi w}} \left(1 - \frac{3}{2}F(|w\mathbf{q}|)\right) \tag{23}$$

$$V_{\perp}(\mathbf{q}) = -2\pi D^2 |\mathbf{q}| e^{-|\mathbf{q}|^d}, \tag{24}$$

where  $F(x) = \sqrt{\pi/2}x[1 - \text{Erf}(x/\sqrt{2})]e^{x^2/2}$  with  $\text{Erf}(x)$  the error function. We have assumed that only the ground-state of the optical lattice potential that creates the 2D geometry is occupied and we denote the transverse width by  $w$ . For the interlayer interaction we use the strict 2D limit result which is a very good approximation for the values  $w \leq 0.3d$  to be used below.

## 4.2 Results

From the expression in Eq. (22), it is clear that to obtain the effective interaction of two dimers, one needs the Fourier transform of the coordinate-space wave function squared. In Fig. 6, the effective interaction based on the exact wave function is compared to approximation scheme 2 for a layer width of  $w = 0.1d$ . As expected, the solid and dashed curves are clearly seen to approach each other as  $U$  increases. To explore the effect of the layer width, we plot  $V_{\text{eff}}(k)$  in Fig. 7 for  $U = 5$  and  $10$  for widths  $w = 0.2d$  and  $w = 0.3d$ . The agreement of the exact and approximate solution is striking except for  $U = 5$  and  $w = 0.3d$  where the Gaussian wave function seems to somewhat underestimate the attraction at large  $kd$ . Note that for the physics to remain effectively 2D, we must have  $kw \ll 1$  or  $kd \ll d/w$ . The range becomes smaller at larger  $w$  and at large  $kd$  the results are strongly modified by the 3D dipolar physics.

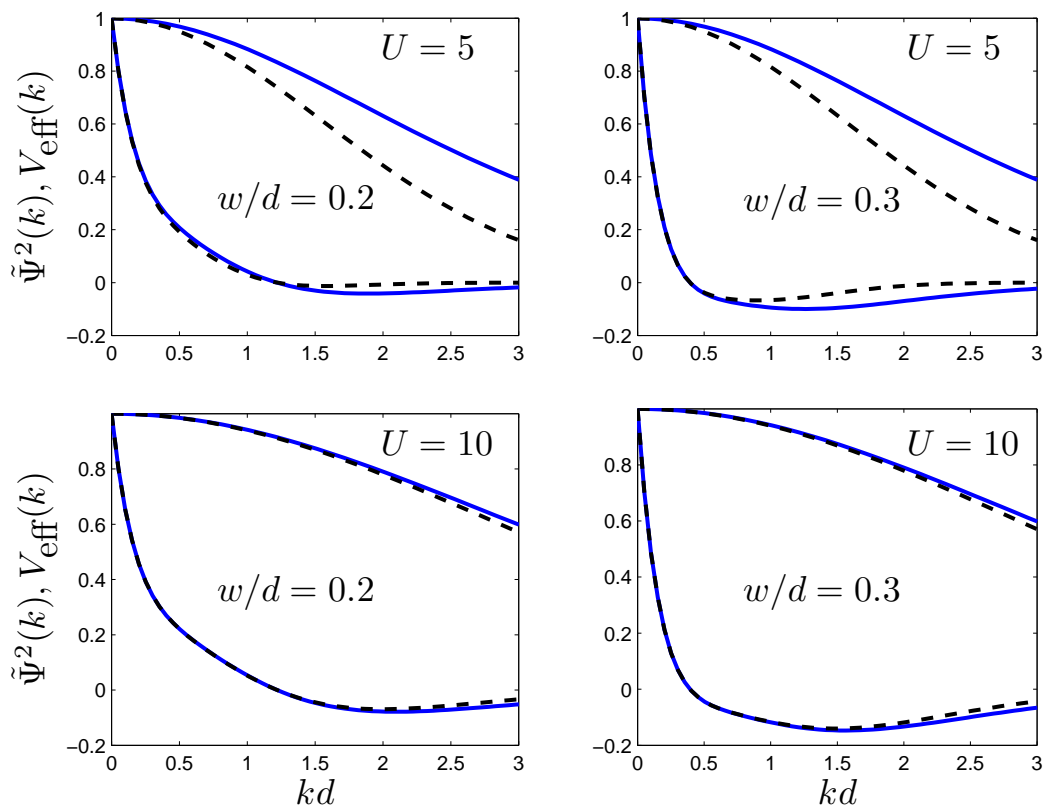


**Fig. 7** (color online) Same as Fig. 6 but with layer widths  $w/d = 0.2$  (left panels) and  $w/d = 0.3$  (right panels) for  $U = 5$  (upper panels) and  $U = 10$  (lower panels).

We have demonstrated that the Gaussian approximation in scheme 2 is accurate at large  $U$ . In particular, this was the limit in which this approximation was used in [32] to calculate properties of the dimerized system at both zero and finite temperature. Furthermore, it is clear that this fact holds for a range of layer sizes, and the Gaussian approximation can be used to study the behavior of the roton instability of a bosonic dimer system that should emerge in the strong-coupling large  $U$  limit. The use of softer lattices that have larger  $w$  implies more attraction at large  $kd$  and the roton instability could become accessible at lower  $U$  values.

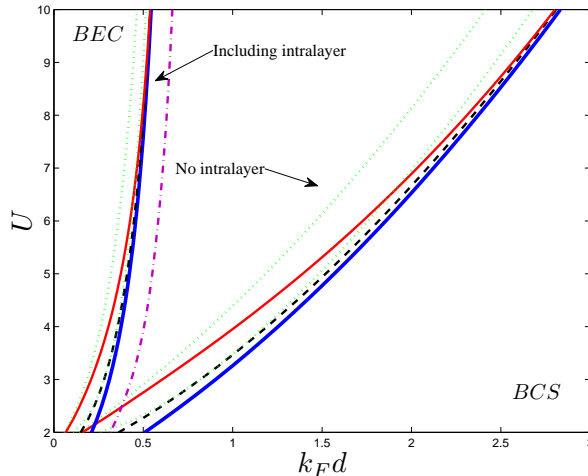


**Fig. 8** (color online) Zero-temperature phase diagram with lines of vanishing chemical potential both with and without including the intralayer interaction as discussed in the text. Results based on the exact energy are shown as the thick solid (blue) line. Also shown energies based on the the variationally optimized Gaussian (dashed (black) line), scheme 2 (solid (ref) line), and scheme 3 (dotted (green) lines). For comparison, the dash-dotted (purple) line to the right of the lines marked 'Including intralayer' shows the result of a calculation of the crossover using the BCS gap equation including the self-energy term self-consistently (taken from [32]). It demonstrates the good agreement between BCS (traditionally weak-coupling theory) and the strong-coupling approach discussed in the current presentation. All calculations use  $w/d = 0.2$ .

## 5 Many-body Physics

We now consider the many-body physics of the bilayer at intermediate to strong coupling where the BCS-BEC crossover is expected to happen. As discussed in the introduction, the two-component Fermi gas in 2D with zero-range interactions in the BCS approximation has a closed analytical solution [43, 44, 45]

$$\Delta = \sqrt{2E_F E_B} \quad (25)$$

$$\tilde{\mu} = E_F - \frac{1}{2}E_B, \quad (26)$$

where  $\Delta$  is the constant energy gap,  $\tilde{\mu}$  the chemical potential (recall that  $\mu$  is reserved for the reduced mass),  $E_F = \hbar^2 k_F^2 / 2M$  the Fermi energy, and  $E_B$  the binding energy of the two-body bound state that the attractive zero-range potential supports. We define the crossover from weak-coupling BCS behavior to a two-body bound state BEC as the point where  $\tilde{\mu} = 0$ . If we write  $E_B = \hbar^2 / Ml^2$ , with  $l$  the size of the bound state, then  $\tilde{\mu} = 0$  occurs when  $2\pi n l^2 = 1$ , i.e. when the inter particle distance is roughly the size of the bound state. In our case with a bilayer of dipolar fermions, we expect these conclusions to be modified by the fact that we have long-range interactions that are both attractive and repulsive.

From a Fermi liquid theory point of view, one could argue that since the long-range dipolar interaction is present on both side of the crossover, it provides a constant shift of the chemical potential and a modification of the effective mass entering the two-body bound that cancel each other and have no influence on the position where the crossover is expected. While this would be correct for small  $U$ , we are here considering the strong-coupling limit and this conclusion may no longer be true. In fact, recent studies have found that other many-body phases in the system such as the density-wave state are very strongly influence by the self-energy correction which drives the instability to larger values of  $U$  [30, 35, 58, 60, 59, 61, 62]. We expect qualitatively similar behaviour in relation to the pairing properties of the system. We therefore consider the problem from the strong-coupling point of view via an effective dimer approach.

In a first approximation, we discard the intralayer interaction and consider the  $\tilde{\mu} = E_F - \frac{1}{2}|E_0| = 0$  line with  $E_0$  the binding energy of the bound state caused by the interlayer potential. Lines of vanishing

$\tilde{\mu}$  can be seen to the right in Fig. 8 for the exact result and the different approximations to the binding energy. Except for scheme 3, the approximations are all very close the exact result, which is not surprising since the approximations are in one way or another derived from the demand that the size of the bound state is close to the exact result.

The intralayer interaction must of course be taken into account, in particular in the strong-coupling regime. One way to proceed is to calculate the effective mass,  $m^*$  and replace  $m \rightarrow m^*$  in  $E_F$  as discussed above. This can be easily done in the weak-coupling regime where the result is analytic [34, 62, 63]. However, we are interested in the strongly-coupled regime where we expect the dimer to be strongly bound and hence the relevant degree of freedom. We therefore consider instead the physics of an interacting Bose gas of two-body bound states for which the chemical potential to lowest order in many-body perturbation theory is  $\tilde{\mu} = \frac{1}{2}nV_{\text{eff}}(0)$  [64]. The factor of one-half is needed since we are interested in the chemical potential per molecule and not per dimer.

In order to include the intralayer interaction we consider now the chemical potential

$$\tilde{\mu} = E_F + \frac{1}{2}nV_{\text{eff}}(0) - \frac{1}{2}|E_0|. \quad (27)$$

The lines where this expression vanishes are shown on the left side of Fig. 8. Clearly the extra repulsion at long distances (small  $kd$ ) pushes the chemical potential up and for the binding energy to compensate this effect we need larger  $U$ , i.e. the lines are pushed to the left to low densities. Again we see that the exact result and the approximations for the binding energy are very close. In Fig. 8 we have used  $w = 0.2d$ . Using a smaller  $w$  will move the lines even further left and vice versa for larger  $w$ . Tuning  $w$  could therefore be a necessary and convenient way to enlarge the BEC regime for experimental access.

For comparison, we also show in Fig. 8 a calculation of the line of vanishing chemical potential using BCS theory, i.e. by solving the gap equations including both inter- and intralayer interactions as discussed in Ref. [32]. It is shown as a (purple) dash-dotted line on the right side of the strong-coupling approach including the intralayer term. The lines show that one finds agreement between the BCS approach and the strong-coupling approach discussed in the current paper. This suggests that the inclusion of the intralayer interaction through the  $nV_{\text{eff}}(0)$  term in the strong-coupling expression of Eq. (27) is consistent with the BCS result. Note that the intralayer interaction is included self-consistently in the BCS equation with the full momentum-dependent potential [32]. The intralayer interaction indeed modifies the BCS phase and not merely by a shift of the chemical potential proportional to  $nV_{\text{eff}}(0)$ .

The use of lowest order perturbation theory to include the intralayer interaction (recall that the interlayer interaction is zero at long wavelength) corresponds to using the first Born approximation. This approximation traditionally fails in the strong-coupling regime. However, the crossover physics of interest happens at low density and we expect the first Born approximation to be reasonable. The perturbative parameter here is  $Uk_Fd$  which must be small. This is true in our phase diagram for  $U \lesssim 5$ . However, the interlayer interaction that is responsible for the bound-state is taken into account essentially exactly through the integration over the bound-state wave function in Eq. (22). We therefore expect our results to still be at least qualitatively correct for larger  $U$  as well.

### 5.1 Pauli Blocking Effect

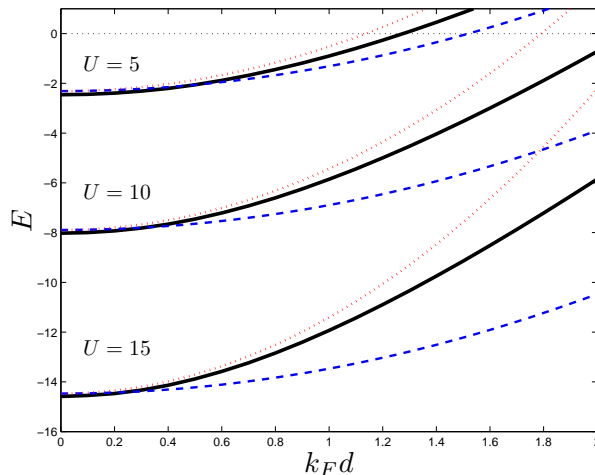
The above discussion was based on a binding energy for the dimer calculated from the pure two-body Schrödinger equation. The fact that the dimer must form in the proximity of other fermionic molecules was taken into account by adding the Fermi energy and the intralayer repulsion. We now proceed by a different route in order to the background Fermi sea into account when forming the dimer. This can be seen as a 'top-down' approach, where the Fermi sea is considered a background on top of which a dimer forms. In contrast, a 'bottom-up' approach would have to consider the full  $N$ -body problem which is a much more difficult task. Our approach is the same as that used to demonstrate the binding of Cooper pairs in the case of short-range interactions for two particles in the presence of Fermi seas. Here it is known to be beneficial to have the background, but this it is not a priori clear that the same holds with long-range dipolar interactions. Below, we calculate the energy in the presence of Fermi seas and show that the energy of the dimer goes up as the Fermi sea is increased. Thus taking the Pauli blocking effect into account to lowest order implies that the crossover could move in the phase

diagram. Notice that we have a Fermi sea background for *both* molecules that form the dimer. This is different from the polaron problem where only one of the particles has a background sea. Interestingly, the polaron problem in the bilayer setup with polar molecules has recently been studied by Klauwunn and Recati [65].

Consider the momentum-space two-body Schrödinger equation

$$\frac{\hbar^2 \mathbf{k}^2}{2\mu} \tilde{\Psi}(\mathbf{k}) + \int \frac{d^2 \mathbf{q}}{(2\pi\hbar)^2} V_{\perp}(\mathbf{k} - \mathbf{q}) \tilde{\Psi}(\mathbf{q}) = E \tilde{\Psi}(\mathbf{k}), \quad (28)$$

where  $\mathbf{k}$  is the relative momentum, which can be solved by discretization. We now include the effect of the background Fermi sea on the dimer by blocking all states with momenta less than the Fermi wave vector  $k_F$ , i.e. we assume that  $\tilde{\Psi}(\mathbf{k}) = 0$  for  $|\mathbf{k}| \leq k_F$ . We also assume that the dimer has zero center-of-mass momentum with respect to the Fermi sea, i.e.  $\mathbf{k}_1 = -\mathbf{k}_2$  so that the relative momentum becomes the lab momentum. Here we are effectively assuming that the Fermi sea is inert in the sense that we neglect particle-hole pairs induced by the interactions. These correlations can be taken into account for instance through the variational ansatz employed for highly polarized Fermi gases with short-range interactions [66], suitably modified to the case of a balanced system which is what we are concerned with here. This will be explored in future work.



**Fig. 9** (color online) Dimer binding energy in units of  $\hbar^2/Md^2$  for  $U = 5, 10,$  and  $15$  as function of  $k_F d$ . The solid (black) curve is the result of solving the momentum-space Schrödinger equation with all states below  $k_F$  blocked. The dashed (blue) curve is the binding energy obtained by using a variationally optimized Gaussian without blocking plus twice the Fermi energy (according to Eq. (29)), while the dotted (red) curve includes twice the Fermi energy and also the lowest-order correction to the potential energy at finite  $k_F$ , Eq. (32).

Before we discuss the numerical results, some limiting analytical expression can be obtained. Let us assume a Gaussian wave function which is a very good approximation for large  $U$ . Then the kinetic energy,  $T$ , in the Pauli blocked case is

$$\frac{\langle \Psi | T | \Psi \rangle}{\langle \Psi | \Psi \rangle} = \frac{\hbar^2}{2\mu b^2} [1 + (k_F b)^2], \quad (29)$$

where  $b$  is the length scale of the Gaussian which can be obtained either variationally or within one of the approximation schemes above. Here we have taken care to re-normalize the wave function when the  $|\mathbf{k}| \leq k_F$  is cut. This is an intuitively pleasing result, and we note that a similar expression can be obtained for the exponential ansatz. The kinetic energy per fermionic molecule can then be written

$$\frac{1}{2} \frac{\langle \Psi | T | \Psi \rangle}{\langle \Psi | \Psi \rangle} = \frac{\hbar^2}{4\mu b^2} + E_F. \quad (30)$$

This should be related to the estimation of the chemical potential through  $\mu = E_F - \frac{1}{2}|E_0|$  as shown on the right of Fig. 8. This approximation corresponds to using Pauli blocking in the kinetic energy while leaving the interaction energy term untouched. The matrix element of the potential in momentum space for the Gaussian wave function is

$$\frac{\langle \Psi | V | \Psi \rangle}{\langle \Psi | \Psi \rangle} = 4\pi b^2 e^{(k_F b)^2} \int_{k_F} \frac{d^2 \mathbf{k}}{(2\pi)^2} e^{-b^2 k^2} \int \frac{d^2 \mathbf{q}}{(2\pi)^2} (-2\pi D^2) q e^{-q d - b^2 q^2 / 2 + b^2 k q \cos \phi_q}, \quad (31)$$

where the factor  $e^{(k_F b)^2}$  comes from the re-normalization of the wave function,  $\langle \Psi | \Psi \rangle = e^{-(k_F b)^2}$ . In the  $k_F \rightarrow 0$  limit, the integral can be performed to yield the total energy given in Eq. (12). The corrections to the potential energy at finite  $k_F$  can be obtained by expansion, which to lowest non-trivial order yields

$$\langle V \rangle = \langle V \rangle_{k_F=0} + \frac{1}{4} \frac{D^2}{d^3} (k_F b)^2 \left( \frac{d}{b} \right)^5 g \left( \frac{b}{d} \right) \quad (32)$$

$$g(y) = -2y + (1 + y^2) \sqrt{2\pi} \text{Erfc} \left[ \frac{1}{\sqrt{2}y} \right] \times \left( \text{Cosh} \left[ \frac{1}{2y^2} \right] + \text{Sinh} \left[ \frac{1}{2y^2} \right] \right). \quad (33)$$

The function  $g(y)$  is positive so that the energy increases with increasing  $k_F$ .

In Fig. 9 we plot the exact solution including Pauli blocking (solid curve) for  $U = 5, 10,$  and  $15$  as a function of  $k_F d$ . As one would expect from the arguments above, the energy increases with  $k_F d$  in a quadratic fashion with a larger slope for larger  $U$ . For comparison, we have also plotted the results of a Gaussian variational calculation of the energy including the effect of blocking on the kinetic energy (dashed (blue) curve) and on both the kinetic and potential energy terms (dotted (red) curve). Recall again that the effect of blocking on the kinetic energy is exact, whereas that on the potential part is only to lowest non-trivial order in  $k_F d$ . The dashed curve in Fig. 9, which includes the blocking in the kinetic energy, overestimates the binding. The inclusion of blocking in the potential (dotted curve in Fig 9) is seen to provide an improvement at small  $k_F d$  (particularly for larger  $U$ ), but still underestimates the binding at large  $k_F d$ . An expansion in large  $k_F d$  can also be done but this is not analytical and provides only limited additional information. We will not pursue this further here.

The fact that decrease of the binding energy with increasing size of the background Fermi sea is faster than predicted by simple addition of the Fermi energy implies that the phase diagram in Fig. 9 must be suitably modified to account for the background effects. Fig. 10 presents a comparison of the lines of vanishing chemical potential when including the Pauli blocking through the exact solution of the momentum-space Schrödinger equation, both with and without including the effects of the intralayer interaction in the long-wavelength limit through addition of  $\frac{1}{2}nV_{\text{eff}}(0)$ . This implies that the background environment reduces the importance of the dimer for the many-body physics.

## 6 Conclusion and Outlook

We have considered a bilayer system with fermionic polar molecules and in particular the two-body bound dimer state that the system supports at any dipole strength. The energy and wave function was calculated exactly and compared to various approximation schemes that provide convenient analytical expressions. We demonstrated that for dipole strength  $U > 1$ , a suitably chosen Gaussian provide a very good analytical approximation in both coordinate- and momentum-space. The effective dimer-dimer interaction was calculated within the different schemes and also found to be well approximated by using Gaussian two-body wave functions, which can be used, for instance, to study roton instabilities [32]. In conclusion, we find that the Gaussian choice is both an accurate and a convenient one due to its simple analytical properties.

The corresponding many-body physics of the bilayer was studied in the context of the 2D Fermi gas where BCS-BEC crossover has been predicted for short-range interactions in the two-component

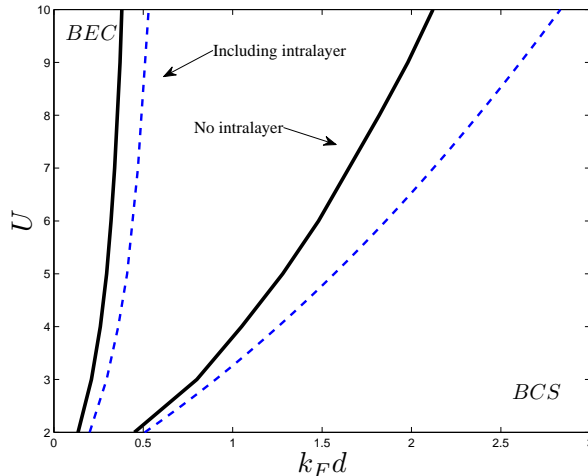


**Fig. 10** (color online) Phase diagram as in Fig. 8. The solid (black) lines obtained from the momentum-space Schrödinger equation including Pauli blocking of low momentum states with (right) and without (left) intralayer interaction, whereas the dashed (blue) lines are obtained by adding the Fermi energy to the unblocked binding energy. The latter corresponds to the solid (blue) lines in Fig. 8. Again we use  $w/d = 0.2$ .

system. This crossover depends sensitively on the two-body bound state. The bilayer system considered in the present paper is very similar since the layer index can be mapped to a spin quantum number. By determining where the chemical potential of the dipolar system vanishes, we could map out a mean-field phase diagram of the BCS and (quasi)-BEC regions. We find this diagram to be largely independent of our approximation schemes for the binding energy. Here we took the effects of the background Fermi sea on the dimer into account both through a simple addition of the Fermi energy, but also by using Pauli blocking of all momenta below the Fermi momentum in the momentum-space Schrödinger equation for the dimer binding energy. This showed that blocking causes a decrease in the binding with the size of the Fermi sea that is faster than naively expected by addition of the Fermi energy to the non-blocked two-body binding energy.

In the bilayer with fermionic polar molecules there are both repulsive and attractive parts. If we neglect the presence of the repulsive intralayer term in the bilayer, we recover the result from the short-range attractive 2D Fermi gas case. However, the long-range intralayer repulsive drastically changes the picture and pushes the BCS-BEC crossover to much smaller densities. This has clear analogs to electron-hole bilayers where the Coulomb interaction provides the long-range part. Here we have included the effect of Pauli blocking on the two-body bound-state energy and demonstrated that this pushes the crossover to even smaller densities, implicating that the BCS paired state occupies the majority of the mean-field phase diagram.

To access the crossover region would require degenerate bilayer systems at very low densities. This is experimentally challenging since the critical temperature of this 2D setup is governed by the BKT transition [67,68]. The transition temperature is proportional to the superfluid density which can be depleted by both interaction and thermal effects. It is therefore driven to very small values at low density. In addition, we need dipole strengths in the range  $U \sim 1 - 10$ , which is higher than current experiments [21]. Using molecules with a larger moment like LiCs or a different optical lattice setup is therefore necessary to probe the crossover. Another possibility is for the system to develop a density wave [29,30,35]. However, strongly bound dimers should change this picture and it is not clear exactly where the density wave transition sits. In any case, we expect it to occupy the large-density and large-strength part of the phase diagram so the crossover physics should be accessible in the low-density and intermediate-strength region.

Two-body states are one important constituent in bilayer system. However,

due to the long-range character of the dipolar interaction, we can have three- or more-body states that are also bound, even though the particles are spatially separated and would not exhibit bound states with zero- or short-range interaction. This is a very interesting feature as it is very different from the paradigmatic crossover BCS-BEC from weakly bound Cooper pairs to strongly bound bosonic two-



body states which is driven by short-range two-body interactions. These questions will be pursued in future investigations.

**Acknowledgements** NTZ gratefully acknowledges numerous discussions with D.-W. Wang and B. Wunsch. This work was supported by the Danish Council for Independent Research | Natural Sciences.

## References

1. Ospelkaus, S. *et al.*: Efficient state transfer in an ultracold dense gas of heteronuclear molecules. *Nature Phys.* **4**, 622 (2008)
2. Ni, K.-K. *et al.*: A High Phase-Space-Density Gas of Polar Molecules. *Science* **322**, 231 (2008)
3. Deiglmayr, J. *et al.*: Formation of Ultracold Polar Molecules in the Rovibrational Ground State. *Phys. Rev. Lett.* **101**, 133004 (2008)
4. Lang, F., Winkler, K., Strauss, C., Grimm, R., Hecker Denschlag, J.: Ultracold Triplet Molecules in the Rovibrational Ground State. *Phys. Rev. Lett.* **101**, 133005 (2008)
5. Carr, L.D., DeMille, D., Kreams, R.V., Ye, J.: Cold and ultracold molecules: science, technology and applications. *New J. Phys.* **11**, 055049 (2009)
6. Ni, K.-K. *et al.*: Dipolar collisions of polar molecules in the quantum regime. *Nature* **464** 1324, (2010)
7. Ospelkaus, S. *et al.*: Quantum-State Controlled Chemical Reactions of Ultracold Potassium-Rubidium Molecules. *Science* **327** 853, (2010)
8. Baranov, M.A.: Theoretical progress in many-body physics with ultracold dipolar gases. *Phys. Rep.* **464**, 71 (2008)
9. Lahaye, T., Menotti, C., Santos, L., Lewenstein, M., Pfau, T.: The physics of dipolar bosonic quantum gases. *Rep. Prog. Phys.* **72**, 126401 (2009)
10. Lushnikov, P.M.: Collapse of Bose-Einstein condensates with dipole-dipole interactions. *Phys. Rev. A* **66**, 051601 (2002)
11. Góral, K., Santos, L., Lewenstein, M.: Quantum Phases of Dipolar Bosons in Optical Lattices. *Phys. Rev. Lett.* **88**, 170406 (2002)
12. DeMille, D.: Quantum Computation with Trapped Polar Molecules. *Phys. Rev. Lett.* **88**, 067901 (2002)
13. Barnett, R., Petrov, D., Lukin, M., Demler, E.: Quantum Magnetism with Multicomponent Dipolar Molecules in an Optical Lattice. *Phys. Rev. Lett.* **96**, 190401 (2006)
14. Micheli, A., Brennen, G.K., Zoller, P.: A toolbox for lattice-spin models with polar molecules. *Nature Phys.* **2**, 341 (2006)
15. Wang, D.-W., Lukin, M.D., Demler, E.: Quantum Fluids of Self-Assembled Chains of Polar Molecules. *Phys. Rev. Lett.* **97**, 180413 (2006)
16. Micheli, A., Pupillo, G., Büchler, H.P., Zoller, P.: Cold polar molecules in two-dimensional traps: Tailoring interactions with external fields for novel quantum phases. *Phys. Rev. A* **76**, 043604 (2007)
17. Büchler, H.P. *et al.*: Strongly Correlated 2D Quantum Phases with Cold Polar Molecules: Controlling the Shape of the Interaction Potential. *Phys. Rev. Lett.* **98**, 060404 (2007)
18. Gorshkov, A.V. *et al.*: Suppression of Inelastic Collisions Between Polar Molecules With a Repulsive Shield. *Phys. Rev. Lett.* **101**, 073201 (2008)
19. Ticknor, C.: Two-dimensional dipolar scattering. *Phys. Rev. A* **80**, 052702 (2009)
20. Micheli, A., Idziaszek, Z., Pupillo, G., Baranov, M.A., Zoller, P., Julienne, P.S.: Universal Rates for Reactive Ultracold Polar Molecules in Reduced Dimensions. *Phys. Rev. Lett.* **105**, 073202 (2010)
21. de Miranda, M.H.G. *et al.*: Controlling the quantum stereodynamics of ultracold bimolecular reactions. *Nature Phys.* **7**, 502 (2011)
22. Wang, D.W.: Quantum Phase Transitions of Polar Molecules in Bilayer . *Phys. Rev. Lett.* **98**, 060403 (2007)
23. Wang, D.W., Demler, E.: Collective excitations and instabilities in multi-layer stacks of dipolar condensates. *arXiv:0812.1838v1*
24. Bruun, G.M., Taylor, E.: Quantum Phases of a Two-Dimensional Dipolar Fermi Gas. *Phys. Rev. Lett.* **101**, 245301 (2008)
25. Lutchyn, R.M., Rossi, E., Das Sarma, S.: Spontaneous interlayer superfluidity in bilayer systems of cold polar molecules. *Phys. Rev. A* **82**, 061604(R) (2010)
26. Cooper, N.R., Shlyapnikov, G.V.: Stable Topological Superfluid Phase of Ultracold Polar Fermionic Molecules. *Phys. Rev. Lett.* **103**, 155302 (2009)
27. Deuretzbacher, F., Cremon, J.C., Reimann, S.M.: Ground-state properties of few dipolar bosons in a quasi-one-dimensional harmonic trap. *Phys. Rev. A* **81**, 063616 (2010)
28. Klawunn, M., Duhme, J., Santos, L.: Bose-Fermi mixtures of self-assembled filaments of fermionic polar molecules. *Phys. Rev. A* **81**, 013604 (2010)
29. Sun, K., Wu, C., Das Sarma, S.: Spontaneous inhomogeneous phases in ultracold dipolar Fermi gases. *Phys. Rev. B* **82**, 075105 (2010)
30. Yamaguchi, Y., Sogo, T., Ito, T., Miyakawa, T.: Density-wave instability in a two-dimensional dipolar Fermi gas. *Phys. Rev. A* **82**, 013643 (2010)
31. Pikovski, A., Klawunn, M., Shlyapnikov, G.V., Santos, L.: Interlayer Superfluidity in Bilayer Systems of Fermionic Polar Molecules. *Phys. Rev. Lett.* **105**, 215302 (2010)

- 
32. Zinner, N.T., Wunsch, B., Pekker, D., Wang, D.W.: BCS-BEC Crossover in Bilayers of Cold Fermionic Polar Molecules. *Phys. Rev. A* **85**, 013603 (2011)
  33. Cremon, J.C., Bruun, G.M., Reimann, S.M.: Tunable Wigner States with Dipolar Atoms and Molecules. *Phys. Rev. Lett.* **105**, 255301 (2010)
  34. Baranov, M.A., Micheli, A., Ronen, S., Zoller, P.: Bilayer superfluidity of fermionic polar molecules: Many-body effects. *Phys. Rev. A* **83**, 043602 (2011)
  35. Zinner, N.T., Bruun, G.M.: Density Waves in Layered Systems with Fermionic Polar Molecules. *Eur. Phys. J. D* **65**, 133 (2011)
  36. Levinsen, J., Cooper, N.R., Shlyapnikov, G.V.: Topological px+ipy superfluid phase of fermionic polar molecules. *Phys. Rev. A* **84**, 013603 (2011)
  37. Ticknor, C., Wilson, R.M., Bohn, J.L.: Anisotropic Superfluidity in a Dipolar Bose Gas. *Phys. Rev. Lett.* **106**, 065301 (2011)
  38. Wunsch, B., Zinner, N.T., Mekhov, I.B., Huang, S.J., Wang, D.W., Demler, E.: Few-body bound states in dipolar gases and their detection. *Phys. Rev. Lett.* **107**, 073201 (2011)
  39. Zinner, N.T., Wunsch, B., Mekhov, I.B., Huang, S.J., Wang, D.W., Demler, E.: Few-Body Bound Complexes in One-dimensional Dipolar Gases and Non-Destructive Optical Detection. *Phys. Rev. A* **84**, 063606 (2011)
  40. Volosniev, A. G., Fedorov, D. V., Jensen, A. S., Zinner, N. T.: Few-body bound state stability of dipolar molecules in two dimensions. arXiv:1109.4602
  41. Huang, S.-J., Hsu, Y.-T., Chen, Y.-C., Volosniev, A.G., Zinner, N.T., Wang, D.-W.: Long-lived supermolecules and their implication to many-body physics. arXiv:1112.2035v1
  42. Fischer, U.R.: Stability of quasi-two-dimensional Bose-Einstein condensates with dominant dipole-dipole interactions. *Phys. Rev. A* **73**, 031602(R) (2006)
  43. Miyake, K.: Fermi Liquid Theory of Dilute Submonolayer  $^3\text{He}$  on Thin  $^4\text{He}$  II Film – Dimer Bound State and Cooper Pairs. *Prog. Theor. Phys.* **69**, 1794 (1983)
  44. Randeria, M., Duan, J.M., Shieh, L.Y.: Bound states, Cooper pairing, and Bose condensation in two dimensions. *Phys. Rev. Lett.* **62**, 981 (1989).
  45. Randeria, M., Duan, J.M., Shieh, L.Y.: Superconductivity in a two-dimensional Fermi gas: Evolution from Cooper pairing to Bose condensation. *Phys. Rev. B* **41**, 327 (1990)
  46. Landau, L.D., Lifshitz, E.M.: *Quantum Mechanics* (Pergamon Press, Oxford, 1976)
  47. Simon, B.: The bound state of weakly coupled Schrödinger operators in one and two dimensions. *Ann. Phys.* **97**, 279 (1976)
  48. Yudson, V.I., Rozman, M.G., Reineker, P.: Bound states of two particles confined to parallel two-dimensional layers and interacting via dipole-dipole or dipole-charge laws. *Phys. Rev. B* **55**, 5214 (1997)
  49. Shih, S.M., Wang, D.W.: Pseudopotential of an interaction with a power-law decay in two-dimensional systems. *Phys. Rev. A* **79**, 065603 (2009)
  50. Armstrong, J.R., Zinner, N.T., Fedorov, D.V., Jensen, A.S.: Bound states and universality in layers of cold polar molecules. *Europhys. Lett.* **91**, 16001 (2010)
  51. Armstrong, J.R., Zinner, N.T., Fedorov, D.V., Jensen, A.S.: Layers of Cold Dipolar Molecules in the Harmonic Approximation. arXiv:1106.2102v1
  52. Volosniev, A.G., Armstrong, J.R., Fedorov, D.V., Jensen, A.S., Zinner, N.T.: Bound Chains of Tilted Dipoles in Layered Systems. arXiv:1112.2541v1
  53. Armstrong, J.R., Zinner, N.T., Fedorov, D.V., Jensen, A.S.: Thermodynamics of Dipolar Chain Systems. arXiv:1112.6141v2
  54. Fedorov, D.V., Armstrong, J.R., Zinner, N.T., Jensen, A.S.: Weakly bound states of polar molecules in bilayers. *Few-body Syst.* **50**, 417 (2011)
  55. Klawunn, M., Pikoński, A., Santos, L.: Two-dimensional scattering and bound states of polar molecules in bilayers. *Phys. Rev. A* **82**, 044701 (2010)
  56. Volosniev, A.G. *et al.*: Bound dimers in bilayers of cold polar molecules. *J. Phys. B* **44**, 125301 (2011)
  57. Volosniev, A.G., Fedorov, D.V., Jensen, A.S., Zinner, N.T.: Model Independence in Two Dimensions and Polarized Cold Dipolar Molecules. *Phys. Rev. Lett.* **106**, 250401 (2011)
  58. Babadi, M., Demler, E.: Density ordering instabilities of quasi-two-dimensional fermionic polar molecules in single-layer and multi-layer configurations: exact treatment of exchange interactions. *Phys. Rev. B* **84**, 235124 (2011)
  59. Sieberer, L. M., Baranov, M. A.: Collective modes, stability and superfluid transition of a quasi-two-dimensional dipolar Fermi gas. *Phys. Rev. A* **84**, 063633 (2011)
  60. Parish, M. M., Marchetti, F. M.: Density instabilities in a two-dimensional dipolar Fermi gas. arXiv:1109.2464
  61. Block, J. K., Zinner, N. T., Bruun, G. M. In preparation.
  62. Chan, C.K., Wu, C.J., Lee, W.C., Das Sarma, S.: Anisotropic-Fermi-liquid theory of ultracold fermionic polar molecules: Landau parameters and collective modes. *Phys. Rev. A* **81**, 023602 (2010)
  63. Kestner, J.P., Das Sarma, S.: Compressibility, zero sound, and effective mass of a fermionic dipolar gas at finite temperature. *Phys. Rev. A* **82**, 033608 (2010)
  64. Fetter, A.L., Walecka, J.D.: *Quantum Theory of Many-Particle Systems*, McGraw-Hill (San Francisco, 1971)
  65. Klawunn, M., Recati, A.: Fermi polaron in two dimensions: Importance of the two-body bound state. *Phys. Rev. A* **84**, 033607 (2011)
  66. Chevy, F., Mora, C.: Ultra-cold polarized Fermi gases. *Rep. Prog. Phys.* **73**, 112401 (2010)
  67. Berezinskii, V.L.: Destruction of Long-range Order in One-dimensional and Two-dimensional Systems Possessing a Continuous Symmetry Group. II. Quantum Systems. *Sov. Phys. JETP* **34**, 610 (1972)
  68. Kosterlitz, J.M., Thouless, D.J.: The critical properties of the two-dimensional xy model. *J. Phys. C* **6**, 1181 (1973)